# The Shapes and Spins of Kuiper Belt Objects

Lacerda, Pedro

CHAPTER 4

# Analysis of the rotational properties

**ABSTRACT**

We use optical data of 10 Kuiper Belt objects (KBOs) to investigate their rotational properties. Of the 10, three (30%) exhibit light variations with amplitude $\Delta m \geq 0.15$ mag, and 1 out of 10 (10%) has $\Delta m \geq 0.40$ mag, which is in good agreement with previous surveys. These data, in combination with the existing database, are used to discuss the rotational periods, shapes, and densities of Kuiper Belt objects. We find that, in the sampled size range, Kuiper Belt objects have a higher fraction of low amplitude lightcurves and rotate slower than main belt asteroids. The data also show that the rotational properties and the shapes of KBOs depend on size. If we split the database of KBO rotational properties into two size ranges with diameter *larger* and *smaller* than 400 km, we find that: (1) the mean lightcurve amplitudes of the two groups are different with 98.5% confidence, (2) the corresponding power-law shape distributions are different, and (3) the two groups occupy different regions on a *spin period* vs. *lightcurve amplitude* diagram. These differences are interpreted in the context of KBO collisional evolution.

Pedro Lacerda and Jane Luu
*to be submitted to Icarus*

## 4.1 Introduction

The Kuiper Belt (KB) is an assembly of small icy objects, orbiting the Sun beyond Neptune. Kuiper Belt objects (KBOs) are likely to be remnants of outer solar system planetesimals (Jewitt & Luu 1993). Their physical, chemical, and dynamical properties should therefore provide valuable information regarding both the environment and the physical processes responsible for planet formation.

At the time of writing, 763 KBOs are known, with 363 of them having been followed for more than one opposition. A total of $\approx 10^5$ objects larger than 50 km are thought to orbit the Sun beyond Neptune (Jewitt & Luu 2000). Studies of KB orbits has revealed an intricate dynamical structure, with signatures of interactions with Neptune (Malhotra 1995). The size distribution follows a differential power-law of index $q = 4$ for bodies $\gtrsim 50$ km (Trujillo et al. 2001a), becoming slightly shallower at smaller sizes (Bernstein et al. 2004).

KBO colours show a large diversity, from slightly blue to very red (Luu & Jewitt 1996; Tegler & Romanishin 2000; Jewitt & Luu 2001), and seem to correlate with inclination and perihelion distance (e.g., Jewitt & Luu 2001; Doressoundiram et al. 2002; Trujillo & Brown 2002). The few low-resolution optical and near-IR KBO spectra are mostly featureless, with the exception of a weak 2 $\mu$m water ice absorption line present in some of them (Brown et al. 1999; Jewitt & Luu 2001).

About 4% of known KBOs are binaries with separations larger than $0\farcs15$ (Noll et al. 2002). All the observed binaries have primary-to-secondary mass ratios $\approx 1$. Two binary creation models have been proposed. Weidenschilling (2002) favours the idea that binaries form in three-body encounters. This model requires a 100 times denser Kuiper Belt at the epoch of binary formation, and predicts a higher abundance of large separation binaries. The alternative scenario (Goldreich et al. 2002), in which the energy needed to bind the orbits of two approaching bodies is drawn from the surrounding swarm of smaller objects, also requires a much higher density of KBOs than the present, but it predicts a larger fraction of close binaries. Recently, Sheppard & Jewitt (2004) have shown evidence that 2001 $\mathrm{QG}_{298}$ could be a close or contact binary KBO, and estimated the fraction of similar objects in the Belt to be $\sim 10\%$–$20\%$.

Other physical properties of KBOs, such as their shapes, densities, and albedos, are still poorly constrained. This is mainly because KBOs are extremely faint, with mean apparent red magnitude $m_R \sim 23$ (Trujillo et al. 2001b).

The study of KBO rotational properties through time-series broadband optical photometry has proved to be the most successful technique to date to investigate some of these physical properties. Light variations of KBOs are believed to be caused mainly by their aspherical shape: as KBOs rotate in space, their projected cross-sections change, resulting in periodic brightness variations.

One of the best examples to date of a KBO lightcurve—and what can be learned from it—is that of (20000) Varuna (Jewitt & Sheppard 2002). The authors explain the lightcurve of Varuna as a consequence of its elongated shape (axes ratio, $a/b \sim 1.5$). They further argue that the object is centripetally deformed by rotation because of its low density, "rubble pile" structure. The term "rubble pile" is generally used to refer to gravitationally bound aggregates of smaller fragments. The existence of rubble piles is thought to be due to continuing mutual collisions throughout the age of the solar system, which gradually fracture the interiors of objects. Rotating rubble piles can adjust their shapes to balance centripetal acceleration and self-gravity. The resulting equilibrium shapes have been studied in the extreme case of fluid bodies, and depend on the body's density and spin rate (Chandrasekhar 1969).

Lacerda & Luu (2003, hereafter LL03a) showed that under reasonable assumptions the fraction of KBOs with detectable lightcurves can be used to constrain the shape distribution of these objects. A follow-up (Luu & Lacerda 2003, hereafter LL03b) on this work, using a database of lightcurve properties of 33 KBOs (Sheppard & Jewitt 2002, 2003), shows that although most Kuiper Belt objects ($\sim 85\%$) have shapes that are close to spherical ($a/b \leq 1.5$) there is a significant fraction ($\sim 12\%$) with highly aspherical shapes ($a/b \geq 1.7$).

In this paper we use optical data of 10 KBOs to investigate the amplitudes and periods of their lightcurves. These data are used in combination with the existing database to investigate the distributions of KBO spin periods and shapes. We discuss their implications for the inner structure and collisional evolution of objects in the Kuiper Belt.

## 4.2 Observations and Photometry

We collected time-series optical data of 10 KBOs at the Isaac Newton 2.5m (INT) and William Herschel 4m (WHT) telescopes. The INT Wide Field Camera (WFC) is a mosaic of 4 EEV 2048×4096 CCDs, each with a pixel scale of $0\farcs33$/pixel and spanning approximately $11\farcm3 \times 22\farcm5$ in the plane of the sky. The targets are imaged through a Johnson R filter. The WHT prime focus camera consists of 2 EEV 2048×4096 CCDs with a pixel scale of $0\farcs24$/pixel, and covers a sky-projected area of $2 \times 8\farcm2 \times 16\farcm4$. With this camera we used a Harris R filter. The seeing for the whole set of observations ranged from 1.0 to 1.9″FWHM. We tracked both telescopes at sidereal rate and kept integration times for each object sufficiently short to avoid errors in the photometry due to trailing effects (see Table 4.1). No light travel time corrections have been made.

We reduced the data using standard techniques. The sky background in the flat-fielded images shows variations of less than 1% across the chip. Background variations between consecutive nights were less than 5% for most of the data. Cosmic rays were removed with the package LA-Cosmic (van Dokkum 2001).

**Table 4.1** – Observing Conditions and Geometry

| Object | Designation | ObsDate[a] | Tel.[b] | Seeing[c] [″] | MvtRt[d] [″/hr] | ITime[e] [sec] | RA[f] [hhmmss] | dec[g] [°′″] | $R^h$ [AU] | $\Delta^i$ [AU] | $\alpha^j$ [deg] |
|---|---|---|---|---|---|---|---|---|---|---|---|
| (19308) | 1996 $TO_{66}$ | 01-Oct-99 | WHT | 1.8 | 2.89 | 500 | 23 59 46 | +03 36 42 | 45.950 | 44.958 | 0.1594 |
| | 1996 $TS_{66}$ | 30-Sep-99 | WHT | 1.3 | 2.62 | 400,600 | 02 26 06 | +21 41 03 | 38.778 | 37.957 | 0.8619 |
| | 1996 $TS_{66}$ | 01-Oct-99 | WHT | 1.1 | 2.67 | 600 | 02 26 02 | +21 40 50 | 38.778 | 37.948 | 0.8436 |
| | 1996 $TS_{66}$ | 02-Oct-99 | WHT | 1.5 | 2.70 | 600,900 | 02 25 58 | +21 40 35 | 38.778 | 37.939 | 0.8225 |
| (35671) | 1998 $SN_{165}$ | 29-Sep-99 | WHT | 1.5 | 3.24 | 360,400 | 23 32 46 | −01 18 15 | 38.202 | 37.226 | 0.3341 |
| (35671) | 1998 $SN_{165}$ | 30-Sep-99 | WHT | 1.4 | 3.22 | 360 | 23 32 41 | −01 18 47 | 38.202 | 37.230 | 0.3594 |
| (19521) | Chaos | 01-Oct-99 | WHT | 1.0 | 1.75 | 360,400,600 | 03 44 37 | +21 30 58 | 42.399 | 41.766 | 1.0616 |
| (19521) | Chaos | 02-Oct-99 | WHT | 1.5 | 1.79 | 400,600 | 03 44 34 | +21 30 54 | 42.399 | 41.755 | 1.0484 |
| | 1999 $DF_9$ | 13-Feb-01 | WHT | 1.7 | 3.19 | 900 | 10 27 04 | +09 45 16 | 39.782 | 38.818 | 0.3124 |
| | 1999 $DF_9$ | 14-Feb-01 | WHT | 1.6 | 3.21 | 900 | 10 26 50 | +09 46 25 | 39.783 | 38.808 | 0.2436 |
| | 1999 $DF_9$ | 15-Feb-01 | WHT | 1.4 | 3.22 | 900 | 10 26 46 | +09 46 50 | 39.783 | 38.806 | 0.2183 |
| | 2000 $CM_{105}$ | 11-Feb-01 | WHT | 1.5 | 3.14 | 600,900 | 09 18 48 | +19 41 59 | 41.753 | 40.774 | 0.1687 |
| | 2000 $CM_{105}$ | 13-Feb-01 | WHT | 1.4 | 3.12 | 900 | 09 18 39 | +19 42 40 | 41.753 | 40.778 | 0.2084 |
| | 2000 $CM_{105}$ | 14-Feb-01 | WHT | 1.5 | 3.11 | 900 | 09 18 34 | +19 43 02 | 41.753 | 40.781 | 0.2303 |
| | 1999 $RZ_{253}$ | 11-Sep-01 | INT | 1.9 | 2.86 | 600 | 22 02 57 | −12 31 06 | 40.963 | 40.021 | 0.4959 |
| | 1999 $RZ_{253}$ | 12-Sep-01 | INT | 1.4 | 2.84 | 600 | 22 02 53 | −12 31 26 | 40.963 | 40.026 | 0.5156 |
| | 1999 $RZ_{253}$ | 13-Sep-01 | INT | 1.8 | 2.82 | 600 | 22 02 49 | −12 31 49 | 40.963 | 40.033 | 0.5381 |
| (47171) | 1999 $TC_{36}$ | 11-Sep-01 | INT | 1.9 | 3.85 | 600 | 00 16 49 | −07 34 59 | 31.416 | 30.440 | 0.4605 |
| (47171) | 1999 $TC_{36}$ | 12-Sep-01 | INT | 1.4 | 3.86 | 900 | 00 16 45 | −07 35 33 | 31.416 | 30.437 | 0.4359 |
| (47171) | 1999 $TC_{36}$ | 13-Sep-01 | INT | 1.8 | 3.88 | 900 | 00 16 39 | −07 36 13 | 31.416 | 30.434 | 0.4122 |
| (38628) | Huya | 28-Feb-01 | INT | 1.5 | 2.91 | 600 | 13 31 13 | −00 39 04 | 29.769 | 29.021 | 1.2725 |
| (38628) | Huya | 01-Mar-01 | INT | 1.8 | 2.97 | 360 | 13 31 09 | −00 38 23 | 29.768 | 29.009 | 1.2479 |
| (38628) | Huya | 03-Mar-01 | INT | 1.5 | 3.08 | 360 | 13 31 01 | −00 36 59 | 29.767 | 28.987 | 1.1976 |
| | 2001 $CZ_{31}$ | 01-Mar-01 | INT | 1.3 | 2.72 | 600,900 | 09 00 03 | +16 29 23 | 41.394 | 40.522 | 0.6525 |
| | 2001 $CZ_{31}$ | 03-Mar-01 | INT | 1.4 | 2.65 | 600,900 | 08 59 54 | +16 30 04 | 41.394 | 40.539 | 0.6954 |

[a] UT date of observation; [b] Telescope used for observations; [c] Average seeing of the data [″]; [d] Average rate of motion of KBO [″/hr]; [e] Integration times used; [f] Right ascension; [g] Declination; [h] KBO–Sun distance; [i] KBO–Earth distance; [j] Phase angle (Sun–Object–Earth angle) of observation.

| Object | Designation | Class[a] | $H^b$ [mag] | $i^c$ [deg] | $e^d$ | $a^e$ [AU] |
|---|---|---|---|---|---|---|
| (19308) | $1996\,TO_{66}$ | C | 4.5 | 27.50 | 0.12 | 43.20 |
| | $1996\,TS_{66}$ | C | 6.4 | 7.30 | 0.13 | 44.00 |
| (35671) | $1998\,SN_{165}$ | C[1] | 5.8 | 4.60 | 0.05 | 37.80 |
| (19521) | Chaos | C | 4.9 | 12.00 | 0.11 | 45.90 |
| | $1999\,DF_{9}$ | C | 6.1 | 9.80 | 0.15 | 46.80 |
| | $2000\,CM_{105}$ | C | 6.2 | 3.80 | 0.07 | 42.50 |
| | $1999\,RZ_{253}$ | C | 5.9 | 0.60 | 0.09 | 43.60 |
| (47171) | $1999\,TC_{36}$ | Pb | 4.9 | 8.40 | 0.22 | 39.30 |
| (38628) | Huya | P | 4.7 | 15.50 | 0.28 | 39.50 |
| | $2001\,CZ_{31}$ | C | 5.4 | 10.20 | 0.12 | 45.60 |

**Table 4.2** – Properties of Observed KBOs. [a]Dynamical class (C = classical KBO, P = Plutino, b = binary KBO); [b]Absolute magnitude; [c]Orbital inclination; [d]Orbital eccentricity; [e]Semi-major axis.

We performed aperture photometry on all objects in the field using the SExtractor software package (Bertin & Arnouts 1996). This software performs circular aperture measurements on each object in a frame, and puts out a catalog of both the magnitudes and the associated errors. Below we describe how we obtained a better estimate of the errors. We used apertures ranging from 1.5 to 2.0 times the FWHM for each frame and selected the aperture that maximized signal-to-noise. An extra aperture of 5 FWHMs was used to look for possible seeing dependent trends in our photometry. The catalogs were matched by selecting only the objects that are present in all frames. The slow movement of KBOs from night to night allows us to successfully match a large number of stars in consecutive nights. We discarded all saturated objects as well as those identified to be galaxies.

The KBO lightcurves were obtained from differential photometry with respect to the brightest non-variable field stars. An average of the magnitudes of the brightest stars (the "reference"stars) provides a reference for differential photometry in each frame. This method allows for small amplitude brightness variations to be detected even under non-photometric conditions.

The uncertainty in the relative photometry was calculated from the scatter in the photometry of fainter field stars that are similar to the KBOs in brightness (the "comparison"stars, see Fig.4.1). This error estimate is more robust than the errors provided by SExtractor (see below), and was used to verify the accuracy of the latter. This procedure resulted in consistent time series brightness data for $\sim 100$ objects (KBO + field stars) in a time span of 2–3 consecutive nights.

We observed Landolt standard stars whenever conditions were photometric, and used them to calibrate the zero point of the magnitude scale. The extinction coefficient was obtained from the reference stars.

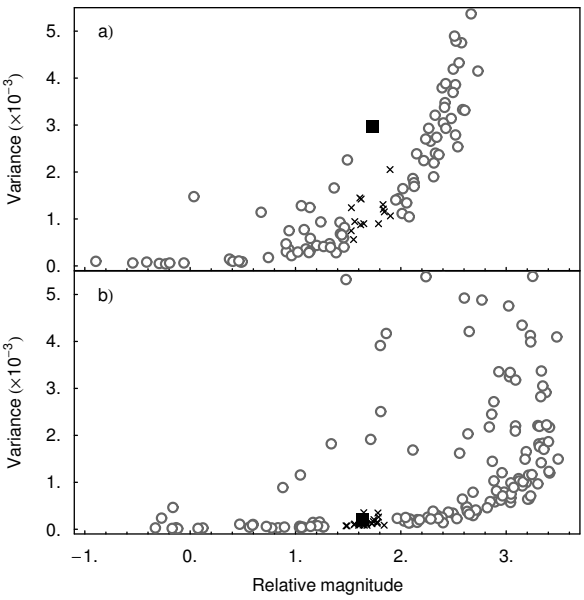


**Figure 4.1** – Frame-to-frame photometric variances of all stars (gray circles and black crosses) in the 1998 $SN_{165}$ (a) and Huya (b) fields, plotted against their relative magnitude. The trend of increasing photometric variability with increasing magnitude is clear. The intrinsically variable stars clearly do not follow this trend, and are located towards the upper left region of the plot. The KBOs are shown as black squares. 1998 $SN_{165}$, in the top panel shows a much larger variability than the comparison stars (shown as crosses, see Section 4.3.1), while Huya is well within the expected variance range, given its magnitude.

| UT Date | Julian Date | $m_R$ [mag] |
|---|---|---|
| 1999 Oct 1.84831 | 2451453.34831 | 21.24 ± 0.07 |
| 1999 Oct 1.85590 | 2451453.35590 | 21.30 ± 0.07 |
| 1999 Oct 1.86352 | 2451453.36352 | 21.20 ± 0.07 |
| 1999 Oct 1.87201 | 2451453.37201 | 21.22 ± 0.07 |
| 1999 Oct 1.87867 | 2451453.37867 | 21.21 ± 0.07 |
| 1999 Oct 1.88532 | 2451453.38532 | 21.28 ± 0.07 |
| 1999 Oct 1.89302 | 2451453.39302 | 21.27 ± 0.06 |
| 1999 Oct 1.90034 | 2451453.40034 | 21.30 ± 0.06 |
| 1999 Oct 1.90730 | 2451453.40730 | 21.28 ± 0.06 |
| 1999 Oct 1.91470 | 2451453.41470 | 21.31 ± 0.06 |

**Table 4.3** – Photometric measurements of 1996 $TO_{66}$. Columns are UT date at the start of the exposure, Julian date at the start of the exposure, and apparent red magnitude. The errors include the uncertainties in relative and absolute photometry added quadratically.

Since not all nights were photometric the lightcurves are presented as variations with respect to the mean brightness. These yield the correct amplitudes and periods of the lightcurves but do not provide their absolute magnitudes.

The orbital parameters and other properties of the observed KBOs are given in Table 4.2. Tables 4.3, 4.4, 4.5, and 4.6 list the absolute $R$-magnitude photometric measurements obtained for 1996 $TO_{66}$, 1996 $TS_{66}$, 1998 $SN_{165}$, and Chaos, respectively.

## 4.3 Lightcurve Analysis

The results in this paper depend solely on the amplitude and period of the KBO lightcurves. It is therefore important to accurately determine these parameters and the associated uncertainties.

**Table 4.4** – Photometric measurements of 1996 $TS_{66}$. Columns are UT date at the start of the exposure, Julian date at the start of the exposure, and apparent red magnitude. The errors include the uncertainties in relative and absolute photometry added quadratically.

| UT Date | Julian Date | $m_R$ [mag] |
|---|---|---|
| 1999 Sep 30.06087 | 2451451.56087 | 21.94 ± 0.07 |
| 1999 Sep 30.06628 | 2451451.56628 | 21.83 ± 0.07 |
| 1999 Sep 30.07979 | 2451451.57979 | 21.76 ± 0.07 |
| 1999 Sep 30.08529 | 2451451.58529 | 21.71 ± 0.07 |
| 1999 Sep 30.09068 | 2451451.59068 | 21.75 ± 0.07 |
| 1999 Sep 30.09695 | 2451451.59695 | 21.67 ± 0.07 |
| 1999 Sep 30.01250 | 2451451.60250 | 21.77 ± 0.07 |
| 1999 Sep 30.10936 | 2451451.60936 | 21.76 ± 0.06 |
| 1999 Sep 30.11705 | 2451451.61705 | 21.80 ± 0.06 |
| 1999 Sep 30.12486 | 2451451.62486 | 21.77 ± 0.06 |
| 1999 Sep 30.13798 | 2451451.63798 | 21.82 ± 0.07 |
| 1999 Sep 30.14722 | 2451451.64722 | 21.74 ± 0.06 |
| 1999 Sep 30.15524 | 2451451.65524 | 21.72 ± 0.06 |
| 1999 Sep 30.16834 | 2451451.66834 | 21.72 ± 0.08 |
| 1999 Sep 30.17680 | 2451451.67680 | 21.83 ± 0.07 |
| 1999 Sep 30.18548 | 2451451.68548 | 21.80 ± 0.06 |
| 1999 Sep 30.19429 | 2451451.69429 | 21.74 ± 0.07 |
| 1999 Sep 30.20212 | 2451451.70212 | 21.78 ± 0.07 |
| 1999 Sep 30.21010 | 2451451.71010 | 21.72 ± 0.07 |
| 1999 Sep 30.21806 | 2451451.71806 | 21.76 ± 0.09 |
| 1999 Sep 30.23528 | 2451451.73528 | 21.73 ± 0.07 |
| 1999 Sep 30.24355 | 2451451.74355 | 21.74 ± 0.08 |
| 1999 Oct 01.02002 | 2451452.52002 | 21.81 ± 0.06 |
| 1999 Oct 01.02799 | 2451452.52799 | 21.82 ± 0.06 |
| 1999 Oct 01.03648 | 2451452.53648 | 21.81 ± 0.06 |
| 1999 Oct 01.04422 | 2451452.54422 | 21.80 ± 0.06 |
| 1999 Oct 01.93113 | 2451453.43113 | 21.71 ± 0.06 |
| 1999 Oct 01.94168 | 2451453.44168 | 21.68 ± 0.06 |
| 1999 Oct 01.95331 | 2451453.45331 | 21.73 ± 0.06 |
| 1999 Oct 01.97903 | 2451453.47903 | 21.69 ± 0.06 |
| 1999 Oct 01.99177 | 2451453.49177 | 21.74 ± 0.06 |
| 1999 Oct 02.00393 | 2451453.50393 | 21.73 ± 0.05 |
| 1999 Oct 02.01588 | 2451453.51588 | 21.78 ± 0.05 |
| 1999 Oct 02.02734 | 2451453.52734 | 21.71 ± 0.05 |

### 4.3.1 Can we detect the KBO brightness variation?

We begin by investigating if the observed brightness variations are intrinsic to the KBO, i.e., if the KBOs intrinsic brightness variations are detectable given our uncertainties. This was done by comparing the frame-to-frame scatter in the KBO optical data with that of ($\sim 10 - 20$) comparison stars.

To visually compare the scatter in the magnitudes of the reference stars (see Section 4.2), comparison stars, and KBOs, we plot a histogram of their frame-to-frame variances (see Fig. 4.2). In general such a histogram should show the reference stars clustered at the lowest variances, followed by the comparison stars spread over larger variances. If the KBO appears isolated at much higher variances than both groups of stars (e.g., Fig. 4.2-j), then its brightness modulations are significant. Conversely, if the KBO is clustered with the stars (e.g. Fig. 4.2-f), any periodic brightness variations would be below the detection threshold.

Figure 4.1 shows the dependence of the uncertainties on magnitude. Objects that do not fall on the rising curve traced out by the stars must have intrin-

| UT Date | Julian Date | $m_R$ [mag] |
|---|---|---|
| 1999 Sep 29.87384 | 2451451.37384 | 21.20 ± 0.06 |
| 1999 Sep 29.88050 | 2451451.38050 | 21.19 ± 0.05 |
| 1999 Sep 29.88845 | 2451451.38845 | 21.18 ± 0.05 |
| 1999 Sep 29.89811 | 2451451.39811 | 21.17 ± 0.05 |
| 1999 Sep 29.90496 | 2451451.40496 | 21.21 ± 0.05 |
| 1999 Sep 29.91060 | 2451451.41060 | 21.24 ± 0.05 |
| 1999 Sep 29.91608 | 2451451.41608 | 21.18 ± 0.05 |
| 1999 Sep 29.92439 | 2451451.42439 | 21.25 ± 0.05 |
| 1999 Sep 29.93055 | 2451451.43055 | 21.24 ± 0.05 |
| 1999 Sep 29.93712 | 2451451.43712 | 21.26 ± 0.06 |
| 1999 Sep 29.94283 | 2451451.44283 | 21.25 ± 0.06 |
| 1999 Sep 29.94821 | 2451451.44821 | 21.28 ± 0.06 |
| 1999 Sep 29.96009 | 2451451.46009 | 21.25 ± 0.06 |
| 1999 Sep 29.96640 | 2451451.46640 | 21.21 ± 0.06 |
| 1999 Sep 29.97313 | 2451451.47313 | 21.17 ± 0.05 |
| 1999 Sep 29.97850 | 2451451.47850 | 21.14 ± 0.05 |
| 1999 Sep 29.98373 | 2451451.48373 | 21.12 ± 0.06 |
| 1999 Sep 29.98897 | 2451451.48897 | 21.15 ± 0.06 |
| 1999 Sep 29.99469 | 2451451.49469 | 21.15 ± 0.06 |
| 1999 Sep 29.99997 | 2451451.49997 | 21.16 ± 0.06 |
| 1999 Sep 30.00521 | 2451451.50521 | 21.12 ± 0.06 |
| 1999 Sep 30.01144 | 2451451.51144 | 21.09 ± 0.06 |
| 1999 Sep 30.02164 | 2451451.52164 | 21.18 ± 0.06 |
| 1999 Sep 30.02692 | 2451451.52692 | 21.17 ± 0.06 |
| 1999 Sep 30.84539 | 2451452.34539 | 21.32 ± 0.06 |
| 1999 Sep 30.85033 | 2451452.35033 | 21.30 ± 0.06 |
| 1999 Sep 30.85531 | 2451452.35531 | 21.28 ± 0.06 |
| 1999 Sep 30.86029 | 2451452.36029 | 21.31 ± 0.06 |
| 1999 Sep 30.86550 | 2451452.36550 | 21.21 ± 0.06 |
| 1999 Sep 30.87098 | 2451452.37098 | 21.26 ± 0.06 |
| 1999 Sep 30.87627 | 2451452.37627 | 21.28 ± 0.06 |
| 1999 Sep 30.89202 | 2451452.39202 | 21.23 ± 0.05 |
| 1999 Sep 30.89698 | 2451452.39698 | 21.30 ± 0.06 |
| 1999 Sep 30.90608 | 2451452.40608 | 21.20 ± 0.05 |
| 1999 Sep 30.91191 | 2451452.41191 | 21.26 ± 0.05 |
| 1999 Sep 30.92029 | 2451452.42029 | 21.15 ± 0.05 |
| 1999 Sep 30.92601 | 2451452.42601 | 21.19 ± 0.05 |
| 1999 Sep 30.93110 | 2451452.43110 | 21.14 ± 0.05 |
| 1999 Sep 30.93627 | 2451452.43627 | 21.16 ± 0.05 |
| 1999 Sep 30.94858 | 2451452.44858 | 21.18 ± 0.05 |
| 1999 Sep 30.95363 | 2451452.45363 | 21.16 ± 0.05 |
| 1999 Sep 30.95852 | 2451452.45852 | 21.13 ± 0.05 |
| 1999 Sep 30.96347 | 2451452.46347 | 21.17 ± 0.05 |
| 1999 Sep 30.96850 | 2451452.46850 | 21.16 ± 0.05 |
| 1999 Sep 30.97422 | 2451452.47422 | 21.18 ± 0.05 |
| 1999 Sep 30.98431 | 2451452.48431 | 21.18 ± 0.05 |
| 1999 Sep 30.98923 | 2451452.48923 | 21.17 ± 0.06 |
| 1999 Sep 30.99444 | 2451452.49444 | 21.16 ± 0.05 |
| 1999 Sep 30.99934 | 2451452.49934 | 21.20 ± 0.05 |
| 1999 Oct 01.00424 | 2451452.50424 | 21.16 ± 0.05 |
| 1999 Oct 01.00992 | 2451452.50992 | 21.18 ± 0.06 |

**Table 4.5** – Photometric measurements of $1998\,SN_{165}$. Columns are UT date at the start of the exposure, Julian date at the start of the exposure, and apparent red magnitude. The errors include the uncertainties in relative and absolute photometry added quadratically.

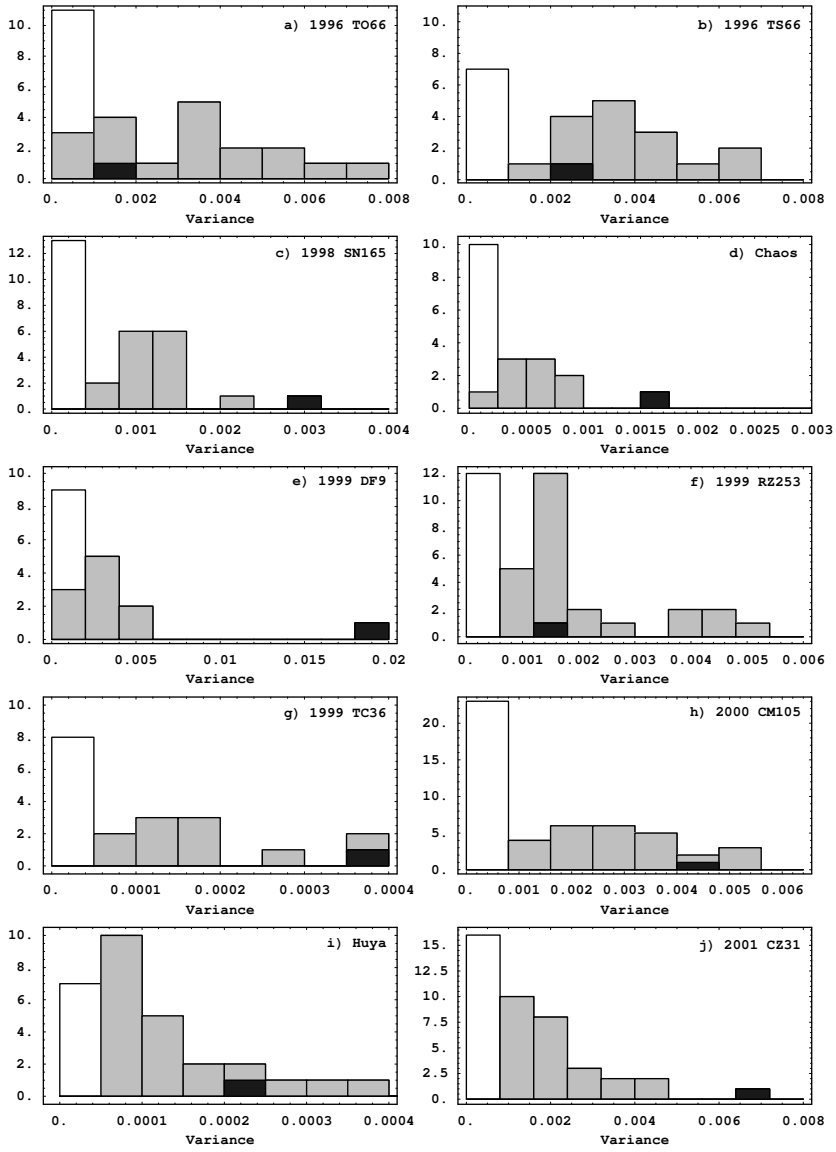


**Figure 4.2** – Stacked histograms of the frame-to-frame variance in the optical data of the "reference" stars (in white), "comparison" stars (in gray), and the KBO (in black). In c), e), and j) the KBO shows significantly more variability than the comparison stars, whereas in all other cases it falls well within the range of photometric uncertainties of the stars of similar brightness.

| UT Date | Julian Date | $m_R$ [mag] |
|---|---|---|
| 1999 Oct 01.06329 | 2451452.56329 | 20.82 ± 0.06 |
| 1999 Oct 01.06831 | 2451452.56831 | 20.80 ± 0.06 |
| 1999 Oct 01.07324 | 2451452.57324 | 20.80 ± 0.06 |
| 1999 Oct 01.07817 | 2451452.57817 | 20.81 ± 0.06 |
| 1999 Oct 01.08311 | 2451452.58311 | 20.80 ± 0.06 |
| 1999 Oct 01.08801 | 2451452.58801 | 20.76 ± 0.06 |
| 1999 Oct 01.09370 | 2451452.59370 | 20.77 ± 0.06 |
| 1999 Oct 01.14333 | 2451452.64333 | 20.71 ± 0.06 |
| 1999 Oct 01.15073 | 2451452.65073 | 20.68 ± 0.06 |
| 1999 Oct 01.15755 | 2451452.65755 | 20.70 ± 0.06 |
| 1999 Oct 01.16543 | 2451452.66543 | 20.72 ± 0.06 |
| 1999 Oct 01.17316 | 2451452.67316 | 20.72 ± 0.06 |
| 1999 Oct 01.18112 | 2451452.68112 | 20.71 ± 0.06 |
| 1999 Oct 01.18882 | 2451452.68882 | 20.73 ± 0.06 |
| 1999 Oct 01.19652 | 2451452.69652 | 20.70 ± 0.06 |
| 1999 Oct 01.20436 | 2451452.70436 | 20.69 ± 0.06 |
| 1999 Oct 01.21326 | 2451452.71326 | 20.72 ± 0.06 |
| 1999 Oct 01.21865 | 2451452.71865 | 20.72 ± 0.06 |
| 1999 Oct 01.22402 | 2451452.72402 | 20.74 ± 0.06 |
| 1999 Oct 01.22938 | 2451452.72938 | 20.72 ± 0.06 |
| 1999 Oct 01.23478 | 2451452.73478 | 20.71 ± 0.07 |
| 1999 Oct 01.24022 | 2451452.74022 | 20.72 ± 0.07 |
| 1999 Oct 02.04310 | 2451453.54310 | 20.68 ± 0.06 |
| 1999 Oct 02.04942 | 2451453.54942 | 20.69 ± 0.06 |
| 1999 Oct 02.07568 | 2451453.57568 | 20.74 ± 0.07 |
| 1999 Oct 02.08266 | 2451453.58266 | 20.73 ± 0.06 |
| 1999 Oct 02.09188 | 2451453.59188 | 20.74 ± 0.06 |
| 1999 Oct 02.10484 | 2451453.60484 | 20.75 ± 0.06 |
| 1999 Oct 02.11386 | 2451453.61386 | 20.77 ± 0.06 |
| 1999 Oct 02.12215 | 2451453.62215 | 20.77 ± 0.06 |
| 1999 Oct 02.13063 | 2451453.63063 | 20.78 ± 0.06 |
| 1999 Oct 02.13982 | 2451453.63982 | 20.79 ± 0.06 |
| 1999 Oct 02.14929 | 2451453.64929 | 20.71 ± 0.07 |

**Table 4.6** – Photometric measurements of Chaos. Columns are UT date at the start of the exposure, Julian date at the start of the exposure, and apparent red magnitude. The errors include the uncertainties in relative and absolute photometry added quadratically.

sic brightness variations. By calculating the mean and spread of the variance for the comparison stars (shown as crosses) we can calculate our photometric uncertainties and thus determine whether the KBO brightness variations are significant.

### 4.3.2 Period determination

In the cases where significant brightness variations were detected in the lightcurves, the phase dispersion minimization method was used (PDM, Stellingwerf 1978) to look for periodicities in the data. For each test period PDM computes a statistical parameter $\theta$ that compares the spread of data points in phase bins with the overall spread of the data. The period that best fits the data is the one that minimizes $\theta$. The advantages of PDM are that it is non-parametric, i.e., it does not assume a shape for the lightcurve, and it can handle unevenly spaced data. Each data set was tested for periods ranging from 2 to 24 hours, in steps of 0.01 hr.

**Table 4.7** – Lightcurve Properties of Observed KBOs. [a]Mean red magnitude. Errors include uncertainties in relative and absolute photometry added quadratically; [b]Number of nights with useful data. Numbers in brackets indicate number of nights of data from other observers used for period determination. Data for $1998\,SN_{165}$ taken from Peixinho et al. (2002) and data for $2001\,CZ_{31}$ taken from SJ02; [c]Lightcurve amplitude; [d]Lightcurve period.

| Object | Designation | $m_R$[a] [mag] | Nts[b] | $\Delta m_R$[c] [mag] | $P$[d] [hr] |
|---|---|---|---|---|---|
| (35671) | $1998\,SN_{165}$ | 21.20±0.05 | 2(1) | 0.16±0.01 | 8.84 |
| | $1999\,DF_9$ | – | 3 | 0.40±0.02 | 6.65 |
| | $2001\,CZ_{31}$ | | 2(1) | 0.21±0.02 | 4.71 |
| (19308) | $1996\,TO_{66}$ | 21.26±0.06 | 1 | ? | |
| | $1996\,TS_{66}$ | 21.76±0.05 | 3 | <0.15 | |
| (19521) | Chaos | 20.74±0.06 | 2 | <0.10 | |
| | $2000\,CM_{105}$ | – | 2 | <0.14 | |
| | $1999\,RZ_{253}$ | – | 3 | <0.05 | |
| (47171) | $1999\,TC_{36}$ | – | 3 | <0.07 | |
| (38628) | Huya | – | 2 | <0.04 | |

### 4.3.3 Amplitude determination

We used a Monte Carlo experiment to determine the amplitude of the lightcurves for which a period was found. We generated several artificial data sets by randomizing each point within the error bar. Each artificial data set was fitted with a Fourier series, using the best-fit period, and the mode and central 68% of the distribution of amplitudes were taken as the lightcurve amplitude and $1\sigma$ uncertainty, respectively.

For the "null"lightcurves, i.e. those where no significant variation was detected, we subtracted the typical error bar size from the total amplitude of the data to obtain an upper limit to the amplitude of the KBO photometric variation.

In this section we present the results of the lightcurve analysis for each of the observed KBOs. We found significant brightness variations ($\Delta m > 0.15$ mag) for 3 out of 10 KBOs (30%), and $\Delta m \geq 0.40$ mag for 1 out of 10 (10%). This is consistent with previously published results: SJ02 found a fraction of 31% with $\Delta m > 0.15$ mag and 23% with $\Delta m > 0.40$ mag, both consistent with our results. The other 7 KBOs do not show detectable variations. The results are summarized in Table 4.7.

## 4.4 Results

### 4.4.1 1998 $SN_{165}$

The brightness of $1998\,SN_{165}$ varies significantly ($> 5\sigma$) more than that of the comparison stars (see Figs. 4.1 and 4.2-c). The periodogram for this KBO shows a very broad minimum around $P = 9$ hr (Fig. 4.3a). The degeneracy implied by the broad minimum would only be resolved with additional data. A slight weaker minimum is seen at $P = 6.5$ hr, which is close to a 24hr alias of 9 hr.

Peixinho et al. (2002, hereafter PDR02) observed this object in September 2000, but having only one night's worth of data, they did not succeed in determining this object's rotational period unambiguously. We used their data to solve the degeneracy in our PDM result. The PDR02 data have not been absolutely calibrated, and the magnitudes are given relative to a bright field star. To be able to combine it with our own data we had to subtract the mean magnitudes. Our periodogram of $1998\,SN_{165}$ (centered on the broad minimum) is shown in Fig. 4.3b and can be compared with the revised periodogram obtained with our data combined with the PDR02 data (Fig. 4.3c). The minima become much clearer with the additional data, but because of the 1-year time difference between the two observational campaigns, many close aliases appear in the periodogram. The absolute minimum, at $P = 8.84$ hr, corresponds to a double peaked lightcurve (see Fig. 4.4). The second best fit, $P = 8.7$ hr, produces a more scattered phase plot, in which the peak in the PDR02 data coincides with our night 2. We will use $P = 8.84$ hr in the rest of the paper, as this corresponds to the PDM absolute minimum.

The amplitude, obtained using the Monte Carlo method described in Section 4.3.3, is $\Delta m = 0.16 \pm 0.01$ mag. This value was calculated using only our data, but it did not change when recalculated adding the PDR02 data.

### 4.4.2 1999 $DF_9$

$1999\,DF_9$ shows large amplitude photometric variations ($\Delta m_R \sim 0.4$ mag). The PDM periodogram for $1999\,DF_9$ is shown in Fig. 4.5. The best-fit period is $P = 6.65$ hr, which corresponds to a double-peak lightcurve (Fig. 4.6). Other PDM minima are found close to $P/2 \approx 3.3$ hr and 9.2 hr, a 24 hr alias of the best period. Phasing the data with $P/2$ results in a worse fit because the two minima of the double peaked lightcurve exhibit significantly different morphologies (Fig. 4.6); the peculiar shape of the brighter minimum, which is reproduced on two different nights, may be caused by an effect other than shape, e.g., a darker (lower albedo) region on the KBO's surface.

The amplitude of the lightcurve, estimated as described in Section 4.3.3, is $\Delta m_R = 0.4 \pm 0.02$ mag.

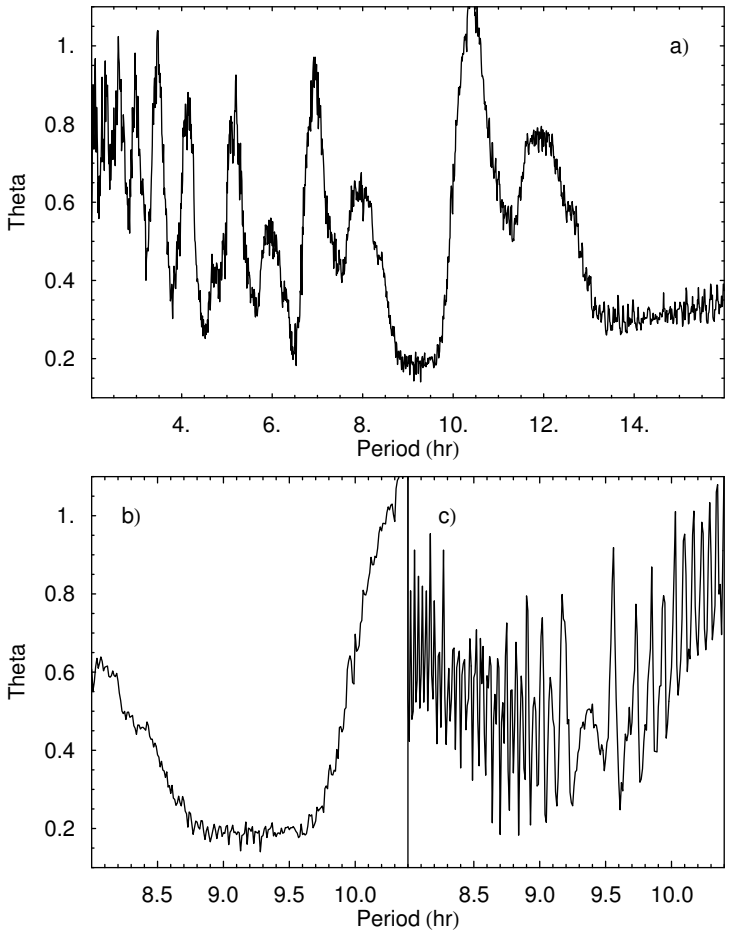


**Figure 4.3** – Periodogram for the data of $1998\,\mathrm{SN}_{165}$. The lower left panel (b) shows an enlarged section near the minimum calculated using only the data published in this paper, and the lower right panel (c) shows the same region recalculated after adding the PDR02 data.

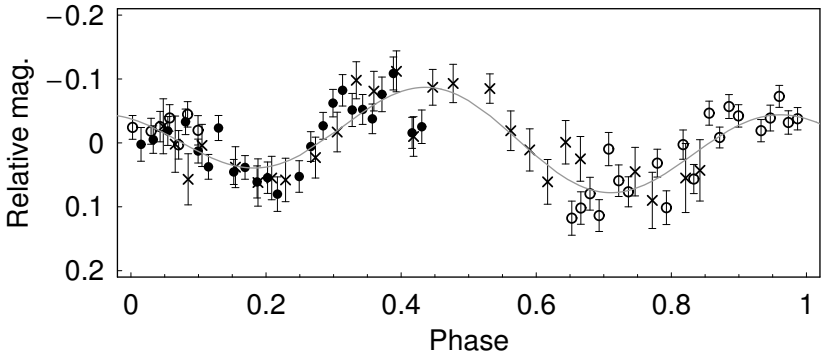


**Figure 4.4** – Lightcurve of $1998\,\mathrm{SN}_{165}$. The figure represents the data phased with the best fit period $P = 8.84\,\mathrm{hr}$. Different symbols correspond to different nights of observation. The gray line is a 2nd order Fourier series fit to the data. The PDR02 data are shown as crosses.

### 4.4.3 2001 $\mathrm{CZ}_{31}$

This object shows substantial brightness variations ($4.5\sigma$ above the comparison stars) in a systematic manner. The first night of data seems to sample nearly one complete rotational phase. As for $1998\,\mathrm{SN}_{165}$, the $2001\,\mathrm{CZ}_{31}$ data span only two nights of observations. In this case, however, the PDM minima (see Figs. 4.7a and 4.7b) are very narrow and only two correspond to independent periods, $P = 4.69\,\mathrm{hr}$ (the minimum at 5.82 is a 24 hr alias of 4.69 hr), and $P = 5.23\,\mathrm{hr}$.

$2001\,\mathrm{CZ}_{31}$ has also been observed by Sheppard & Jewitt (2002, hereafter SJ02) in February and April 2001, with inconclusive results. We used their data to try to rule out one (or both) of the two periods we found. We subtracted the SJ02 mean magnitudes in order to combine it with our uncalibrated observations. Figure 4.7c shows the section of the periodogram around $P = 5\,\mathrm{hr}$, recalculated using SJ02's first night plus our own data. The aliases are due to the 1 month time difference between the two observing runs. The new PDM minimum is at $P = 4.71\,\mathrm{hr}$—very close to the $P = 4.69\,\mathrm{hr}$ determined from our data alone.

Visual inspection of the combined data set phased with $P = 4.71\,\mathrm{hr}$ shows a very good match between SJ02's first night (2001 Feb 20) and our own data (see Fig. 4.8). SJ02's second and third nights show very large scatter and were not included in our analysis. Phasing the data with $P = 5.23\,\mathrm{hr}$ yields a more scattered lightcurve, which confirms the PDM result. We will use $P = 4.71\,\mathrm{hr}$ throughout the rest of the paper.

We measured a lightcurve amplitude of $\Delta m = 0.21 \pm 0.02\,\mathrm{mag}$. If we use both ours and SJ02's first night data, $\Delta m$ rises to 0.22 mag.

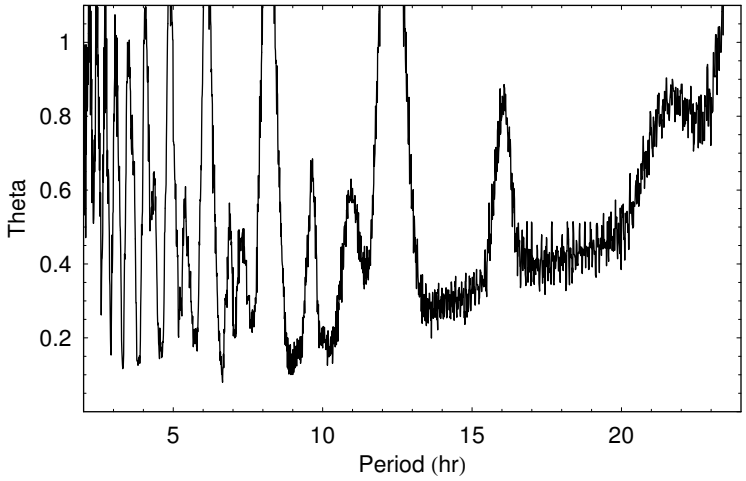


**Figure 4.5** – Periodogram for the 1999 $DF_9$ data. The minimum corresponds to a lightcurve period $P = 6.65$ hr.

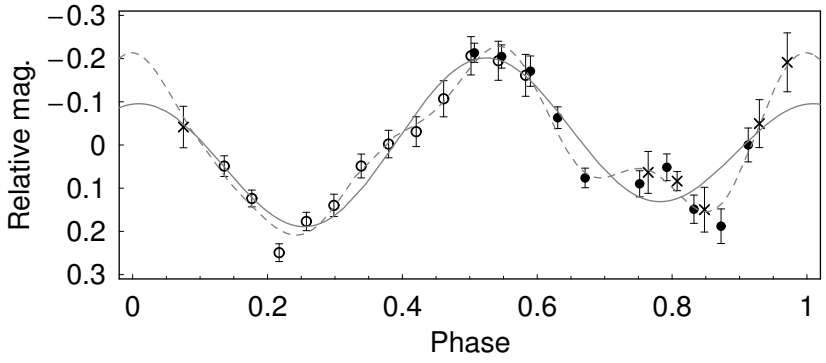


**Figure 4.6** – Same as Figure 4.4 for KBO 1999 $DF_9$. The best fit period is $P = 6.65$ hr. The lines represent a 2nd order (solid line) and 5th (dashed line) order Fourier series fits to the data. Normalized $\chi^2$ values of the fits are 2.8 and 1.3 respectively.

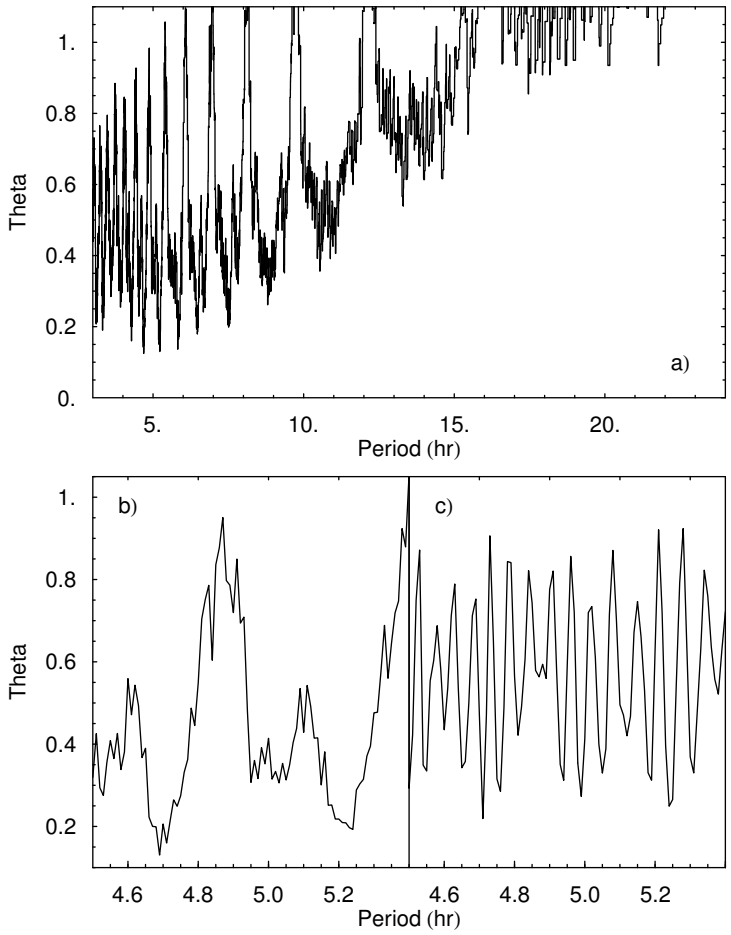


**Figure 4.7** – Periodogram for the 2001 $CZ_{31}$ data. The lower left panel (b) shows an enlarged section near the minimum calculated using only the data published in this paper, and the lower right panel (c) shows the same region recalculated after adding the SJ02 data.

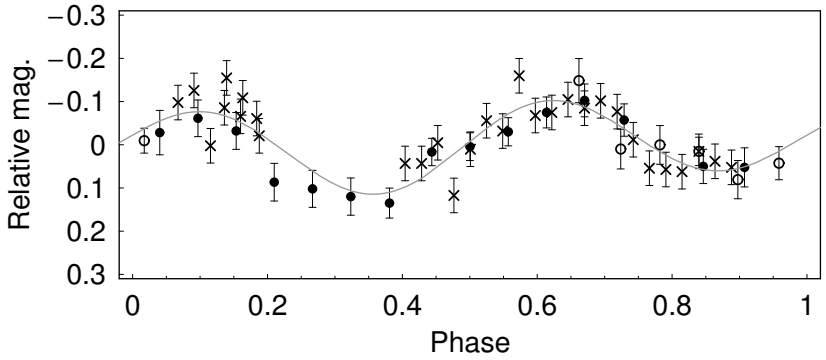


**Figure 4.8** – Same as Figure 4.4 for KBO 2001 $CZ_{31}$. The data are phased with period $P = 4.71$ hr. The points represented by crosses are taken from SJ02.

### 4.4.4 Flat Lightcurves

The fluctuations detected in the optical data of KBOs 1996 $TO_{66}$, 1996 $TS_{66}$, 1999 $TC_{36}$, 1999 $RZ_{253}$, 2000 $CM_{105}$, and Huya, are well within the uncertainties. Chaos shows some variations with respect to the comparison stars but no period was found to fit all the data. See Table 4.7 and Fig. 4.9 for a summary of the results.

### 4.4.5 Other lightcurve measurements

The KBO lightcurve database has increased considerably in the last few years, largely due to the observational campaign of SJ02, with a recent updates in Sheppard & Jewitt (2003, hereafter SJ03) and Sheppard & Jewitt (2004). These authors have published observations and rotational data for a total of 30 KBOs (their SJ02 paper includes data for 3 other previously published lightcurves in the analysis). Other recently published KBO lightcurves include those for (50000) Quaoar (Ortiz et al. 2003) and the scattered KBO (29981) 1999 $TD_{10}$ (Rousselot et al. 2003). Of the 10 KBO lightcurves presented in this paper, 6 are new to the database, bringing the total to 41.

Table 4.8 lists the rotational data of the 41 KBOs that will be analyzed in the rest of the paper.

## 4.5 Analysis

In this section we examine the lightcurve properties of KBOs and compare them with those of main-belt asteroids (MBAs). The lightcurve data for these two families of objects cover different size ranges. MBAs, being closer to Earth, can be observed down to much smaller sizes than KBOs; in general it is very

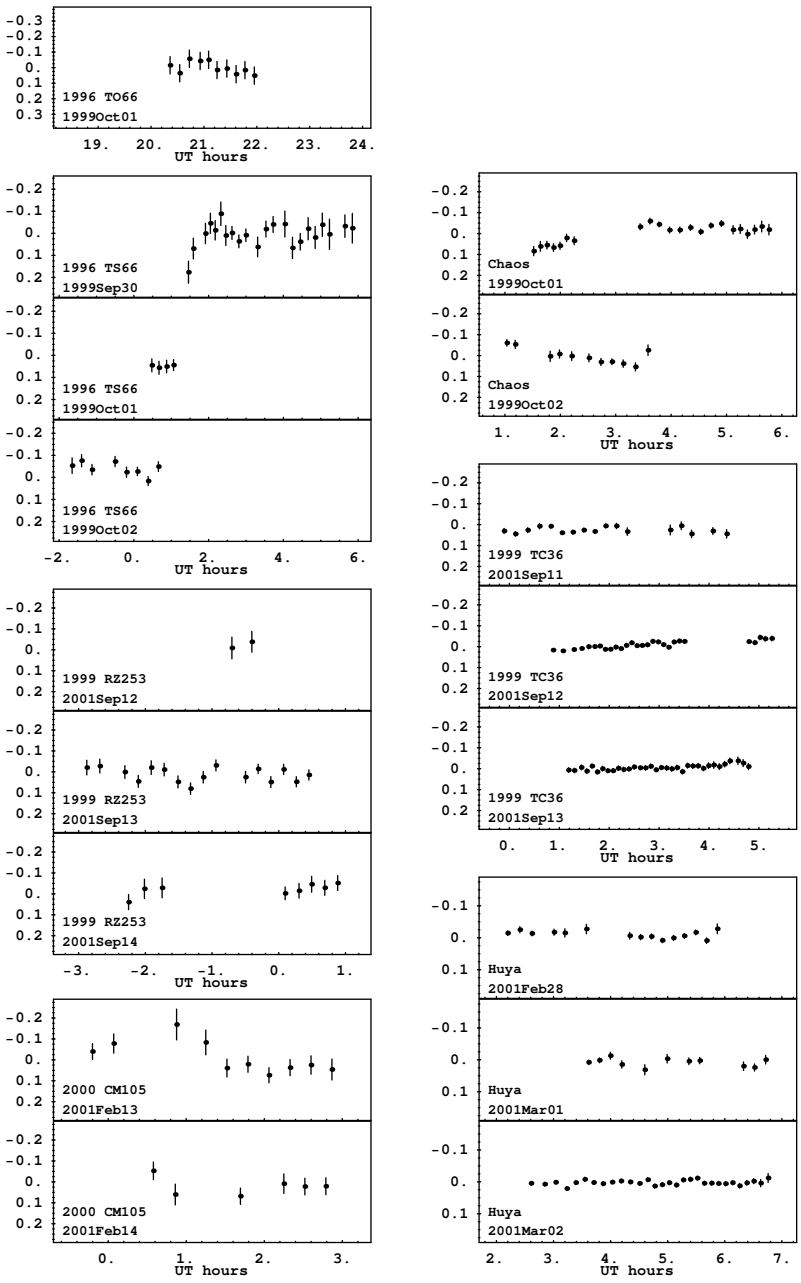


**Figure 4.9** – The "flat" lightcurves are shown. The respective amplitudes are within the photometric uncertainties.

**Table 4.8** – Database of KBOs Lightcurve Properties.

| Object | Designation | Class[a] | Size[b] [km] | Period[c] [hr] | $\Delta m_R$[d] [mag] | Source[e] |
|---|---|---|---|---|---|---|
| | KBOs considered to have $\Delta m < 0.15$ mag | | | | | |
| 15789 | 1993 SC | P | 240 | | 0.04 | RT99, DMcG97 |
| 15820 | 1994 TB | P | 220 | | <0.04 | SJ02 |
| | 1996 $GQ_{21}$ | S | 730 | | <0.10 | SJ02 |
| | 1996 $TL_{66}$ | S | 480 | | 0.06 | RT99, LJ98 |
| 15875 | 1996 $TP_{66}$ | P | 250 | | 0.12 | RT99, CB99 |
| | 1997 $CS_{29}$ | C | 630 | | <0.08 | SJ02 |
| | 1998 $HK_{151}$ | P | 170 | | <0.15 | SJ02 |
| 33340 | 1998 $VG_{44}$ | P | 280 | | <0.10 | SJ02 |
| 19521 | Chaos | C | 600 | | <0.10 | LL, SJ02 |
| | 1999 $DE_9$ | S | 700 | | <0.10 | SJ02 |
| 47171 | 1999 $TC_{36}$ | Pb | 600 | | <0.07 | LL, SJ03 |
| 38628 | Huya | P | 740 | | <0.04 | LL, SJ03 |
| | 2000 $YW_{134}$ | S | 790 | | <0.10 | SJ03 |
| | 2001 $FP_{185}$ | S | 400 | | <0.10 | SJ03 |
| | 2001 $FZ_{173}$ | S | 430 | | <0.06 | SJ02 |
| | 2001 $KD_{77}$ | P | 430 | | <0.10 | SJ03 |
| 28978 | Ixion | P | 1310 | | <0.10 | SJ03, O01 |
| | 2001 $QF_{298}$ | P | 580 | | <0.10 | SJ03 |
| 42301 | 2001 $UR_{163}$ | S | 1020 | | <0.10 | SJ03 |
| 42355 | 2002 $CR_{46}$ | S | 210 | | <0.10 | SJ03 |
| 55636 | 2002 $TX_{300}$ | C | 1250 | 16.24 | 0.08±0.02 | SJ03 |
| 55637 | 2002 $UX_{25}$ | C | 1090 | | <0.10 | SJ03 |
| 55638 | 2002 $VE_{95}$ | P | 500 | | <0.10 | SJ03 |
| | 2000 $CM_{105}$ | C | 330 | | <0.14 | LL |
| | 1999 $RZ_{253}$ | Cb | 380 | | <0.05 | LL |
| | 1996 $TS_{66}$ | C | 300 | | <0.14 | LL |
| | KBOs considered to have $\Delta m \geq 0.15$ mag | | | | | |
| 32929 | 1995 $QY_9$ | P | 180 | 7.3 | 0.60±0.04 | SJ02, RT99 |
| 24835 | 1995 $SM_{55}$ | C | 630 | 8.08 | 0.19±0.05 | SJ03 |
| 19308 | 1996 $TO_{66}$ | C | 720 | 7.9 | 0.26±0.03 | SJ03, H00 |
| 26308 | 1998 $SM_{165}$ | R | 400 | 7.1 | 0.45±0.03 | SJ02, R01 |
| 33128 | 1998 $BU_{48}$ | S | 210 | 9.8 | 0.68±0.04 | SJ02, R01 |
| 40314 | 1999 $KR_{16}$ | C | 400 | 11.858 | 0.18±0.04 | SJ02 |
| 47932 | 2000 $GN_{171}$ | P | 360 | 8.329 | 0.61±0.03 | SJ02 |
| 20000 | Varuna | C | 980 | 6.34 | 0.42±0.03 | SJ02 |
| | 2003 $AZ_{84}$ | P | 900 | 13.44 | 0.14±0.03 | SJ03 |
| | 2001 $QG_{298}$ | Pcb | 240 | 13.7744 | 1.14±0.04 | SJ04 |
| 50000 | Quaoar | C | 1300 | 17.6788 | 0.17±0.02 | O03 |
| 29981 | 1999 $TD_{10}$ | S | 100 | 15.3833 | 0.53±0.03 | Rou03 |
| 35671 | 1998 $SN_{165}$ | C | 400 | 8.84 | 0.16±0.01 | LL |
| | 1999 $DF_9$ | C | 340 | 6.65 | 0.40±0.02 | LL |
| | 2001 $CZ_{31}$ | C | 440 | 4.71 | 0.21±0.06 | LL |

[a]Dynamical class (C = classical KBO, P = Plutino, b = binary KBO).

[b]Diameter in km assuming an albedo of 0.04, except for (20000) Varuna which has a known albedo of 0.07.

[c]Period of the lightcurve in hours. For KBOs with both single and double peaked possible lightcurves the double peaked period is listed.

[d]Lightcurve amplitude in magnitudes.

[e]DMcG97 = Davies et al. (1997), CB99 = Collander-Brown et al. (1999), H00 = Hainaut et al. (2000), LJ98 = Luu & Jewitt (1998), O01 = Ortiz et al. (2001), O03 = Ortiz et al. (2003), RT99 = Romanishin & Tegler (1999), R01 = Romanishin et al. (2001), Rou03 = Rousselot et al. (2003), SJ02 = Sheppard & Jewitt (2002), SJ03 = Sheppard & Jewitt (2003), SJ04 = Sheppard & Jewitt (2004), LL = this work.

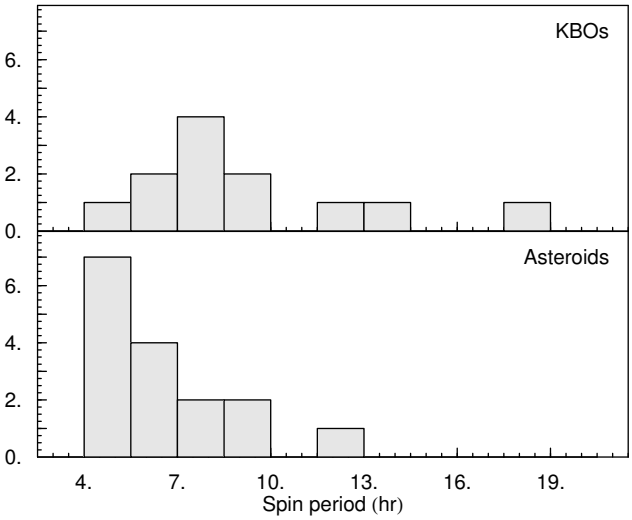


**Figure 4.10** – Histograms of the spin periods of KBOs (upper panel) and main belt asteroids (lower panel) satisfying $D > 200\,\mathrm{km}$, $\Delta m \geq 0.15\,\mathrm{mag}$, $P < 20\,\mathrm{hr}$. The mean rotational periods of KBOs and MBAs are 9.23 hr and 6.48 hr, respectively. The $y$-axis in both cases indicates the number of objects in each range of spin periods.

difficult to obtain good quality lightcurves for KBOs with diameters $D < 50\,\mathrm{km}$. Furthermore, some KBOs surpass the 1000 km barrier—assuming a 0.04 albedo, 5 objects in the current database have diameters in excess of 1000 km—whereas the largest asteroid, Ceres, does not reach 900 km. This will be taken into account in the analysis.

The lightcurve data for asteroids was taken from the Harris Lightcurve Catalog[2], Version 5, while the diameter data were obtained from the Lowell Observatory database of asteroids orbital elements[3]. The sizes of KBOs were calculated from their absolute magnitude assuming an albedo of 0.04, except for Varuna for which simultaneous thermal and optical observations have yielded a red geometric albedo of $0.07^{+0.30}_{-0.17}$ (Jewitt et al. 2001).

### 4.5.1 Spin period statistics

As Fig. 4.10 shows, the spin period distributions of KBOs and MBAs are significantly different. Because the sample of KBOs of small size or large periods is poor, to avoid bias in our comparison we consider only KBOs and MBAs larger than 200 km and with periods below 20 hr. In this range the mean rotational periods of KBOs and MBAs are 9.23 hr and 6.48 hr, respectively, and the two are different with a 98.5% confidence according to Student's $t$-test. However, the different means do not rule that the underlying distributions are the same, and could simply mean than the two sets of data sample the same distribution differently. This is not the case, however, according to the Kolmogorov-Smirnov

[2] `http://pdssbn.astro.umd.edu/sbnhtml/asteroids/colors_lc.html`
[3] `ftp://ftp.lowell.edu/pub/elgb/astorb.html`

(K-S) test, which gives a probability that the periods of KBOs and MBAs are drawn from the same parent distribution of 0.7%.

Although it is clear that KBOs spin slower than asteroids, it is not clear why this is so. If collisions have contributed as significantly to the angular momentum of KBOs as they did for MBAs (Farinella et al. 1982; Catullo et al. 1984), then the observed difference should be related to how these two families react to collision events.

We will address the question of the collisional evolution of KBO spin rates in Chapter 5.

### 4.5.2 Lightcurve amplitudes and the shapes of KBOs

The cumulative distribution of KBO lightcurve amplitudes is shown in Fig. 4.11. It rises very steeply in the low amplitude range, and then becomes shallower reaching large amplitudes. In quantitative terms, $\sim 70\%$ of the KBOs possess $\Delta m < 0.15$ mag, while $\sim 12\%$ possess $\Delta m \geq 0.40$ mag, with the maximum value being $\Delta m = 0.68$ mag. [Note: Fig. 4.11 does not include the KBO 2001 $QG_{298}$ which has a lightcurve amplitude $\Delta m = 1.14 \pm 0.04$ mag, and would further extend the range of amplitudes. We do not include 2001 $QG_{298}$ in our analysis because it is thought to be a contact binary (Sheppard & Jewitt 2004)]. Figure 4.11 also compares the KBO distribution with that of MBAs. The distributions of the two populations are clearly distinct: in the low amplitude range ($\Delta m < 0.15$ mag) the KBO distribution is steeper than the MBA distribution and extends to larger values of $\Delta m$.

Figure 4.12 shows the lightcurve amplitude of KBOs and MBAs plotted against size. KBOs with diameters larger than $D = 400$ km seem to have lower lightcurve amplitudes than KBOs with diameters smaller than $D = 400$ km. Student's $t$-test confirms that the mean amplitudes in each of these two size ranges are different at the 98.5% confidence level. For MBAs the transition is less sharp and seems to occur at a smaller size ($D \sim 200$ km). In the case of asteroids, the accepted explanation is that small bodies ($D \lesssim 100$ km) are fragments of high-velocity impacts (Catullo et al. 1984), whereas their larger counterparts ($D > 200$ km) are not. The lightcurve data of small KBOs are still too sparse to permit a similar analysis.

The distribution of lightcurve amplitudes can be used to infer the shapes of KBOs, if certain reasonable assumptions are made (see, e.g., LL03a). Generally, objects with elongated shapes produce large brightness variations due to their changing projected cross-section as they rotate. Conversely, round objects, or those with the spin axis aligned with the line of sight, produce little or no brightness variations, resulting in "flat" lightcurves. Figure 4.12 shows that the lightcurve amplitudes of KBOs with diameters smaller and larger than $D = 400$ km are significantly different. Does this mean that the shapes of KBOs

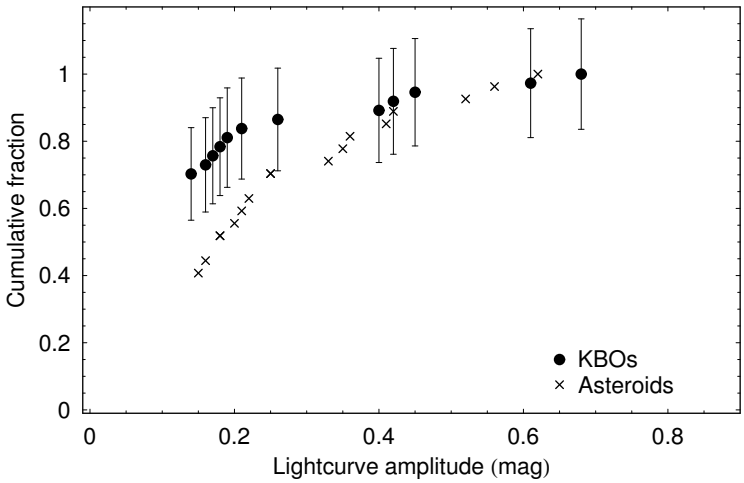


**Figure 4.11** – Cumulative distribution of lightcurve amplitude for KBOs (circles) and asteroids (crosses) larger than 200 km. We plot only KBOs for which a period has been determined. KBO 2001 $QG_{298}$, thought to be a contact binary (Sheppard & Jewitt 2004), is not plotted although it may be considered an extreme case of elongation.

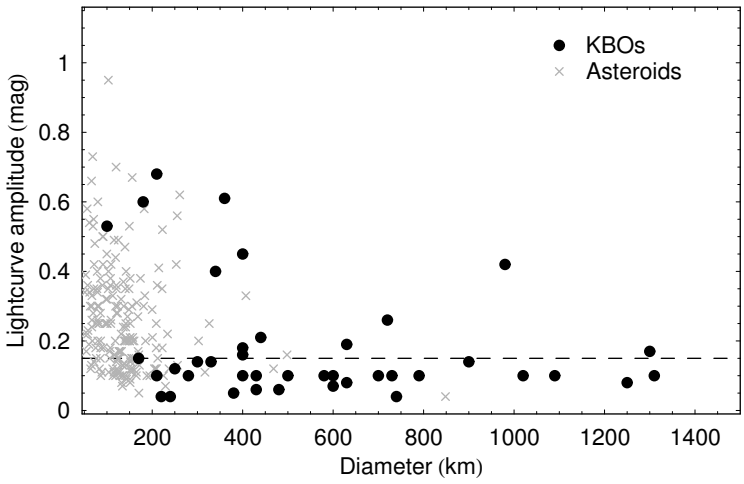


**Figure 4.12** – Lightcurve amplitudes of KBOs (black circles) and main belt asteroids (gray crosses) plotted against object size. All sizes assume albedo of 0.04 except for Varuna, which has a known albedo of 0.07.

are also different in these two size ranges? To investigate this possibility of a size dependence among KBO shapes we will consider KBOs with diameter smaller and larger than 400 km separately. We shall loosely refer to objects with diameter $D > 400$ km and $D \leq 400$ km as *larger* and *smaller* KBOs, respectively.

We approximate the shapes of KBOs by triaxial ellipsoids with semi-axes $a > b > c$. For simplicity we consider the case where $b = c$ and use the axis ratio $\tilde{a} = a/b$ to characterize the shape of an object. The orientation of the spin axis is parameterized by the aspect angle $\theta$, defined as the smallest angular distance between the line of sight and the spin vector. On this basis the lightcurve amplitude $\Delta m$ is related to $\tilde{a}$ and $\theta$ via the relation (Eqn. 2.2 with $\bar{c} = 1$)

$$\Delta m = 2.5 \log \sqrt{\frac{2\,\tilde{a}^2}{1 + \tilde{a}^2 + (\tilde{a}^2 - 1)\,\cos(2\,\theta)}}\ . \tag{4.1}$$

Following LL03b we model the shape distribution by a power-law of the form

$$f(\tilde{a})\,\mathrm{d}\tilde{a} \propto \tilde{a}^{-q}\,\mathrm{d}\tilde{a} \tag{4.2}$$

where $f(\tilde{a})\,\mathrm{d}\tilde{a}$ represents the fraction of objects with shapes between $\tilde{a}$ and $\tilde{a} + \mathrm{d}\tilde{a}$. We use the measured lightcurve amplitudes to estimate the value of $q$ by employing both the method described in LL03a, and by Monte Carlo fitting the observed amplitude distribution (SJ02; LL03b). The latter consists of generating artificial distributions of $\Delta m$ (Eqn. 4.1) with values of $\tilde{a}$ drawn from distributions characterized by different $q$'s (Eqn. 4.2), and selecting the one that best fits the observed cumulative amplitude distribution (Fig. 4.11). The values of $\theta$ are generated assuming random spin axis orientations. We use the K-S test to compare the different fits. The errors are derived by bootstrap resampling the original data set (Efron 1979), and measuring the dispersion in the distribution of best-fit power-law indexes, $q_i$, found for each bootstrap replication.

Following the LL03a method we calculate the probability of finding a KBO with $\Delta m \geq 0.15$ mag:

$$p(\Delta m \geq 0.15) \approx \int_{\sqrt{K}}^{\tilde{a}_{\max}} f(\tilde{a}) \sqrt{\frac{\tilde{a}^2 - K}{(\tilde{a}^2 - 1)K}}\,\mathrm{d}\tilde{a}. \tag{4.3}$$

where $K = 10^{0.8 \times 0.15}$, $f(\tilde{a}) = C\,\tilde{a}^{-q}$, and $C$ is a normalization constant. This probability is calculated for a range of $q$'s to determine the one that best matches the observed fraction of lightcurves with amplitude larger than 0.15 mag. These fractions are $f(\Delta m \geq 0.15\,\mathrm{mag};\ D \leq 400\,\mathrm{km}) = 8/18$, and $f(\Delta m \geq 0.15\,\mathrm{mag};\ D > 400\,\mathrm{km}) = 6/22$, and $f(\Delta m \geq 0.15\,\mathrm{mag}) = 14/40$ for the complete set of data. The results are summarized in Table 4.9 and shown in Fig. 4.13.

Both methods yield steeper shape distributions for larger KBOs, implying more spherical shapes in this size range (Table 4.9). A distribution with $q = 9.8$

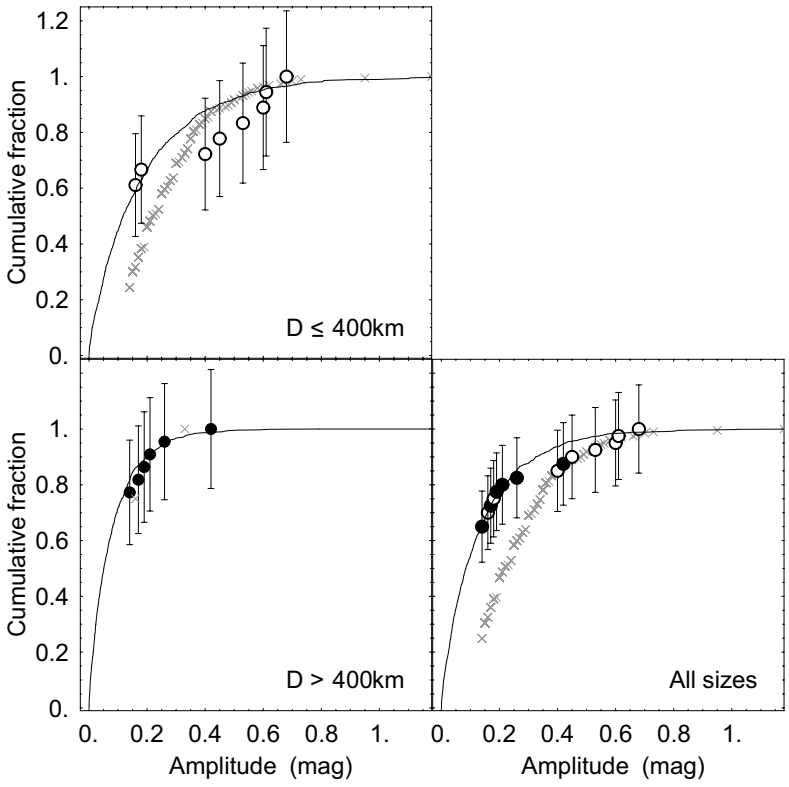


**Figure 4.13** – Observed cumulative lightcurve amplitude distributions of KBOs (black circles) with diameter smaller than 400 km (upper left panel), larger than 400 km (lower left panel), and of all the sample (lower right panel) are shown as black circles. Error bars are poissonian. The best fit power-law shape distributions of the form $f(\tilde{a})\,\mathrm{d}\tilde{a} = \tilde{a}^{-q}\,\mathrm{d}\tilde{a}$ were converted to amplitude distributions using a Monte Carlo technique (see text for details), and are show as solid lines. The best fit $q$'s are listed in Table 4.9. The gray crosses show the distributions for asteroids in the same size ranges.

| Size range | Method LL03 | Method MC |
|---|---|---|
| $D \leq 400\,\mathrm{km}$ | $q = 4.0^{+2.0}_{-1.5}$ | $q = 4.5 \pm 2.3$ |
| $D > 400\,\mathrm{km}$ | $q = 6.7^{+2.7}_{-2.1}$ | $q = 9.8 \pm 2.6$ |
| All sizes | $q = 5.8^{+1.4}_{-1.3}$ | $q = 6.1 \pm 1.7$ |

**Table 4.9** – Best fit parameter to the KBO shape distribution. Column 1 is the range of KBO diameters, in km, considered in each case. Columns 2 and 3 are the results from the method described in LL03, and from a Monte Carlo fit of the lightcurve amplitude distribution, respectively. See text for detailed discussion.

predicts that ∼80% of the large KBOs have $a/b < 1.2$. For the smaller objects we find a shallower distribution, $q \sim 4 - 4.5$, which implies a significant fraction of very elongated objects: $\sim$ 15% have $a/b > 1.7$. Although based on small

numbers, the shape distribution of large KBOs is well fit by a simple power-law (the K-S rejection probability is 0.3%). This is not the case for smaller KBOs for which the fit is poorer (K-S rejection probability is 61%, see Fig. 4.13). Our results are in agreement with previous studies of the overall KBO shape distribution, which had already shown that a simple power-law does not explain the shapes of KBOs as a whole (LL03b; SJ02).

The results presented in this section suggest that the shape distributions of smaller and larger KBOs are different. However, given the size of our sample, we cannot conclusively state that this difference is significant. Better observational contraints, particularly of smaller KBOs, are necessary to understand the origin of the KBO shape distribution. A comparison with asteroids suggests that the collisional evolution may have played an important role. Collisions in the asteroid belt have left different marks in smaller and larger bodies. The shapes of smaller asteroids ($D \leq 100\,\mathrm{km}$) are consistent with collisional fragments (Catullo et al. 1984), indicating that they are most likely by-products of disruptive collisions. Larger asteroids have in principle survived collisional destruction for the age of the solar system, but may nonetheless have been converted to rubble piles by repeated impacts. As a result of multiple collisions, the "loose" pieces of the larger asteroids may have reassembled into shapes close to triaxial equilibrium ellipsoids (Farinella et al. 1981).

### 4.5.3 The inner structure of KBOs

In this section we wish to investigate if the rotational properties of KBOs show any evidence that they have a rubble pile structure; a possible dependence on object size is also investigated.

Figure 4.14 plots the lightcurve amplitudes versus spin periods for the 15 KBOs whose lightcurve amplitudes and spin period are known. Open and filled symbols indicate the KBOs with diameter smaller and larger than $D = 400\,\mathrm{km}$, respectively. Clearly, the smaller and larger KBOs occupy different regions of the diagram. For the larger KBOs (black filled circles) the (small) lightcurve amplitudes are almost independent of the objects' spin periods. In contrast, smaller KBOs span a much broader range of lightcurve amplitudes. Two object objects have very low amplitudes: $1998\,\mathrm{SN}_{165}$ and $1999\,\mathrm{KR}_{16}$, which have diameters $D \sim 400\,\mathrm{km}$ and fall precisely on the boundary of the two size ranges. The remaining objects hint at a trend of increasing $\Delta m$ with lower spin rates. The one exception is $1999\,\mathrm{TD}_{10}$, a Scattered Disk Object ($e = 0.872, a = 95.703\,\mathrm{AU}$) that spends most of its orbit in rather empty regions of space and most likely has a different collisional history.

For comparison, Fig. 4.14 also shows results of N-body simulations of collisions between "ideal" rubble piles (gray filled circles; Leinhardt et al. 2000), and the lightcurve amplitude-spin period relation predicted by ellipsoidal figures of

hydrostatic equilibrium (dashed and dotted lines; Chandrasekhar 1969; Holsapple 2001). The latter is calculated from the equilibrium shapes that rotating uniform fluid bodies assume by balancing gravitational and centrifugal acceleration. The spin rate-shape relation in the case of uniform fluids depends solely on the density of the body. Although fluid bodies behave in many respects differently from rubble piles, they may, as an extreme case, provide insight on the equilibrium shapes of gravitationally bound agglomerates.

The simulations of Leinhardt et al. (2000, hereafter LRQ2000) consist of collisions between agglomerates of small spheres meant to simulate collisions between rubble piles. Each agglomerate consists of $\sim 1000$ spheres, held together by their mutual gravity, and has no initial spin. The spheres are indestructible, have no sliding friction, and have coefficients of restitution of $\sim 0.8$. The bulk density of the agglomerates is $2000\,\mathrm{kg\,m^{-3}}$. The authors collide two equal-size rubble piles for a range of impact velocities and impact parameters. The impact velocities range from $\sim$ zero at infinity to a few times the critical velocity for which the impact energy would exceed the mutual gravitational binding energy of the two rubble piles. The impact geometries range from head-on collisions to grazing impacts. The mass, final spin period, and shape of the *largest remnant* resulting from each collision are registered and presented (see Table 1 of LRQ2000). From their results, we selected the outcomes for which the mass of the largest remnant is equal or larger than the mass of one of the colliding rubble piles, i.e., we selected only accreting outcomes. The spin periods and lightcurve amplitudes that would be generated by such remnants (assuming they are observed equator-on) are plotted in Fig. 4.14 as gray circles. Nine points, resulting from head-on collisions, are not visible because the periods are larger than 19 hr, up to $\sim 650$ hr. Note that the simulated rubble piles have radii of 1 km—much smaller than the sizes of the KBOs in our database. However, since the effects of the collision scale with the ratio of impact energy to gravitational binding energy of the colliding bodies (Benz & Asphaug 1999), the model results should apply to other sizes. Clearly, the LRQ2000 model makes several specific assumptions, and represents one possible idealization of what is usually referred to as "rubble pile". Nevertheless, the results are illustrative of how collisions may affect this type of structures, and are useful for comparison with the KBO data.

The lightcurve amplitudes resulting from the LRQ2000 experiment are relatively small ($\Delta m < 0.25$ mag) for spin periods larger than $P \sim 5.5$ hr (see Fig. 4.14). Objects spinning faster than $P = 5.5$ hr have more elongated shapes, resulting in larger lightcurve amplitudes, up to 0.65 magnitudes. The latter are the result of collisions with higher angular momentum transfer than the former (see Table 1 of LRQ2000). The maximum spin rate attained by the rubble piles, as a result of the collision, is $\sim 4.5$ hr. This is consistent with the maximum spin expected for bodies in hydrostatic equilibrium with the same density as the rubble piles ($\rho = 2000\,\mathrm{kg\,m^{-3}}$; see long-dashed line in Fig. 4.14). The results of LRQ2000 show that collisions between ideal rubble piles can produce elongated

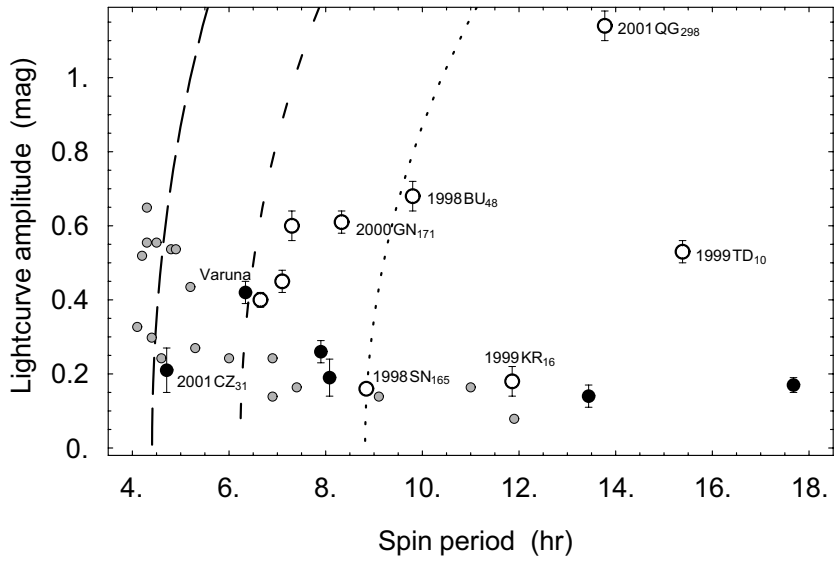


**Figure 4.14** – Lightcurve amplitudes versus spin periods of KBOs. The black filled and open circles represent objects larger and smaller than 400 km, respectively. The smaller gray circles show the results of numerical simulations of "rubble-pile" collisions (Leinhardt et al. 2000). The lines represent the locus of rotating ellipsoidal figures of hydrostatic equilibrium with densities $\rho = 500\,\mathrm{kg\,m^{-3}}$ (dotted line), $\rho = 1000\,\mathrm{kg\,m^{-3}}$ (shorter dashes) and $\rho = 2000\,\mathrm{kg\,m^{-3}}$ (longer dashes). The point towards the upper right corner of the plot corresponds to $2001\,\mathrm{QG_{298}}$ ($P = 13.77\,\mathrm{hr}$, $\Delta m = 1.14\,\mathrm{mag}$), a likely contact binary KBO (Sheppard & Jewitt 2004).

remnants (when the projectile brings significant angular momentum into the target), and that the spin rates of the collisional remnants do not extend much beyond the maximum spin permitted to fluid uniform bodies with the same bulk density.

The distribution of KBOs in Fig. 4.14 is less clear. Indirect estimates of KBO bulk densities indicate values $\rho \sim 1000\,\mathrm{kg\,m^{-3}}$ (Luu & Jewitt 2002). If KBOs are strengthless rubble piles with such low densities we would not expect to find objects with spin periods lower than $P \sim 6\,\mathrm{hr}$ (as indicated by the dashed line in Fig. 4.14). However, one object ($2001\,\mathrm{CZ_{31}}$), is found to have a spin period below 5 hr. If this object has a rubble pile structure, its density must be at least $\sim 2000\,\mathrm{kg\,m^{-3}}$ (see Fig. 4.14). The remaining 14 objects have spin periods below the expected upper limit, given their estimated density. Of the 14, 4 objects lie close to the line corresponding to equilibrium ellipsoids of density $\rho = 1000\,\mathrm{kg\,m^{-3}}$. One of these objects, (20000) Varuna, has been studied in detail by Sheppard & Jewitt (2002). The authors conclude that Varuna is best interpreted as a rotationally deformed rubble pile with $\rho \leq 1000\,\mathrm{kg\,m^{-3}}$. One object, $2001\,\mathrm{QG_{298}}$, has an exceptionally large lightcurve amplitude ($\Delta m = 1.14\,\mathrm{mag}$), indicative of a very elongated shape (axes ratio $a/b > 2.85$). Given

its modest spin rate ($P = 13.8\,\mathrm{hr}$) and approximate size ($D \sim 240\,\mathrm{km}$) it is unlikely that it would be able to keep such an elongated shape against the crush of gravity. Analysis of the lightcurve of this object (Sheppard & Jewitt 2004) suggests it is a contact (or very close) binary KBO. The same applies to two other KBOs, $2000\,\mathrm{GN}_{171}$ and (33128) $1998\,\mathrm{BU}_{48}$, also very likely to be contact binaries.

To summarize, based on the available rotational properties of KBOs, it is not clear if they have a rubble pile structure. Comparing the KBO data with results from computer simulations of rubble pile collisions (LRQ2000) we find that 11 out of 15 ($\sim 73\%$) KBOs have rotational data that follows essentially the same trends as the LRQ2000 results. Of the 11 KBOs, 5 (45%) have diameters $D \leq 400\,\mathrm{km}$, and 6 (55%) have diameters $D > 400\,\mathrm{km}$. If these KBOs are rubble piles then their spin rates set a lower limit to their bulk density: one object ($2001\,\mathrm{CZ}_{31}$) spins fast enough that its density must be at least $\rho \sim 2000\,\mathrm{kg\,m^{-3}}$, while 4 other KBOs (including (20000) Varuna) must have densities larger than $\rho \sim 1000\,\mathrm{kg\,m^{-3}}$. A better assessment of the inner structure of KBOs will require more observations, and detailed modelling of the collisional evolution of rubble-piles.

## 4.6 Conclusions

We have collected and analyzed R-band photometric data for 10 Kuiper Belt objects, 5 of which have not been studied before. No significant brightness variations were detected from KBOs $2000\,\mathrm{CM}_{105}$, $1999\,\mathrm{RZ}_{253}$, $1996\,\mathrm{TS}_{66}$. Previously observed KBOs Chaos, $1999\,\mathrm{TC}_{36}$, and Huya were confirmed to have very low amplitude lightcurves ($\Delta m \leq 0.1\,\mathrm{mag}$). $1998\,\mathrm{SN}_{165}$, $1999\,\mathrm{DF}_{9}$, and $2001\,\mathrm{CZ}_{31}$ were shown to have periodic brightness variations. Our lightcurve amplitude statistics are thus: 3 out of 10 (30%) observed KBOs have $\Delta m \geq 0.15\,\mathrm{mag}$, and 1 out of 10 (10%) has $\Delta m \geq 0.40\,\mathrm{mag}$. This is consistent with previously published results.

The rotational properties that we obtained were combined with existing data in the literature and the total data set was used to investigate the distribution of spin period and shapes of KBOs. Our conclusions can be summarized as follows:

1. KBOs with diameters $D > 200\,\mathrm{km}$ have a mean spin period of 9.23 hr, and thus rotate slower on average than main belt asteroids of similar size ($\langle P \rangle_{\mathrm{MBAs}} = 6.48\,\mathrm{hr}$). The probability that the two distributions are drawn from the same parent distribution is 0.7%.
2. 26 of 37 KBOs (70%, $D > 200\,\mathrm{km}$) have lightcurve amplitudes below 0.15 mag. In the asteroid belt only 10 of the 27 (37%) asteroids in the same size range have such low amplitude lightcurves.
3. KBOs with diameters $D > 400\,\mathrm{km}$ have lightcurves with significantly

(98.5% confidence) smaller amplitudes ($\langle \Delta m \rangle = 0.13\,\mathrm{mag}$, $D > 400\,\mathrm{km}$) than KBOs with diameters $D \leq 400\,\mathrm{km}$ ($\langle \Delta m \rangle = 0.26\,\mathrm{mag}$, $D \leq 400\,\mathrm{km}$).

4. The shape distributions are different for these two size ranges, and predict a larger fraction of round objects in the $D > 400\,\mathrm{km}$ size range ($f(a/b > 1.2) \sim 80\%$) than in the group of smaller objects ($f(a/b > 1.2) \sim 50\%$).
5. The rotational properties of KBOs suggest that some of these objects may have a rubble pile structure: 73% of KBOs with measured spin periods have lightcurve amplitudes and spin periods consistent with rubble piles of density $\rho \gtrsim 1000\,\mathrm{kg\,m^{-3}}$. However, the data are too sparse to allow a conclusive assessment of the inner structure of KBOs.
6. KBO 2001 $\mathrm{CZ}_{31}$ has a spin period of $P = 4.71\,\mathrm{hr}$. If this object has a rubble pile structure then its density must be $\rho \gtrsim 2000\,\mathrm{kg\,m^{-3}}$. If the object has a lower density then it must have internal strength.

## Acknowledgments

This work was supported by grants from the Netherlands Foundation for Research (NWO), and the Leids Kerkhoven-Bosscha Fonds (LKBF). We are grateful to Scott Kenyon and Ivo Labbé for helpful discussion.

## References

Benz, W. & Asphaug, E. 1999, Icarus, 142, 5
Bernstein, G. M., Trilling, D. E., Allen, R. L., Brown, M. E., Holman, M., & Malhotra, R. 2004, AJ, 128, 1364
Bertin, E. & Arnouts, S. 1996, A&AS, 117, 393
Brown, R. H., Cruikshank, D. P., & Pendleton, Y. 1999, ApJ, 519, L101
Catullo, V., Zappala, V., Farinella, P., & Paolicchi, P. 1984, A&A, 138, 464
Chandrasekhar, S. 1969, Ellipsoidal figures of equilibrium (The Silliman Foundation Lectures, New Haven: Yale University Press, 1969)
Collander-Brown, S. J., Fitzsimmons, A., Fletcher, E., Irwin, M. J., & Williams, I. P. 1999, MNRAS, 308, 588
Davies, J. K., McBride, N., & Green, S. F. 1997, Icarus, 125, 61
Dobrovolskis, A. R. & Burns, J. A. 1984, Icarus, 57, 464
Doressoundiram, A., Peixinho, N., de Bergh, C., Fornasier, S., Thébault, P., Barucci, M. A., & Veillet, C. 2002, AJ, 124, 2279
Efron, B. 1979, Annals of Statistics, 7, 1
Farinella, P., Paolicchi, P., Tedesco, E. F., & Zappala, V. 1981, Icarus, 46, 114
Farinella, P., Paolicchi, P., & Zappala, V. 1982, Icarus, 52, 409
Goldreich, P., Lithwick, Y., & Sari, R. 2002, Nature, 420, 643
Hainaut, O. R., Delahodde, C. E., Boehnhardt, H., Dotto, E., Barucci, M. A., Meech, K. J., Bauer, J. M., West, R. M., & Doressoundiram, A. 2000, A&A, 356, 1076
Holsapple, K. A. 2001, Icarus, 154, 432
Jewitt, D., Aussel, H., & Evans, A. 2001, Nature, 411, 446
Jewitt, D. & Luu, J. 1993, Nature, 362, 730
Jewitt, D. C. & Luu, J. X. 2000, Protostars and Planets IV, 1201
—. 2001, AJ, 122, 2099
Jewitt, D. C. & Sheppard, S. S. 2002, AJ, 123, 2110
Lacerda, P. & Luu, J. 2003, Icarus, 161, 174
Leinhardt, Z. M., Richardson, D. C., & Quinn, T. 2000, Icarus, 146, 133
Luu, J. & Jewitt, D. 1996, AJ, 112, 2310
Luu, J. X. & Jewitt, D. C. 2002, ARA&A, 40, 63
Luu, J. & Lacerda, P. 2003, Earth Moon and Planets, 92, 221
Luu, J. X. & Jewitt, D. C. 1998, ApJ, 494, L117+
Noll, K. S., Stephens, D. C., Grundy, W. M., Millis, R. L., Spencer, J., Buie, M. W., Tegler, S. C., Romanishin, W., & Cruikshank, D. P. 2002, AJ, 124, 3424
Ortiz, J. L., Gutiérrez, P. J., Sota, A., Casanova, V., & Teixeira, V. R. 2003, A&A, 409, L13
Ortiz, J. L., Lopez-Moreno, J. J., Gutierrez, P. J., & Baumont, S. 2001, Bulletin of the American Astronomical Society, 33, 1047
Peixinho, N., Doressoundiram, A., & Romon-Martin, J. 2002, New Astronomy, 7, 359
Romanishin, W. & Tegler, S. C. 1999, Nature, 398, 129
Romanishin, W., Tegler, S. C., Rettig, T. W., Consolmagno, G., & Botthof, B. 2001, Bulletin of the American Astronomical Society, 33, 1031
Rousselot, P., Petit, J.-M., Poulet, F., Lacerda, P., & Ortiz, J. 2003, A&A, 407, 1139
Sheppard, S. S. & Jewitt, D. C. 2002, AJ, 124, 1757
—. 2003, Earth Moon and Planets, 92, 207
Sheppard, S. S. & Jewitt, D. 2004, AJ, 127, 3023

Stellingwerf, R. F. 1978, ApJ, 224, 953
Tegler, S. C. & Romanishin, W. 2000, Nature, 407, 979
Trujillo, C. A., Jewitt, D. C., & Luu, J. X. 2001a, AJ, 122, 457
Trujillo, C. A., Luu, J. X., Bosh, A. S., & Elliot, J. L. 2001b, AJ, 122, 2740
Trujillo, C. A. & Brown, M. E. 2002, ApJ, 566, L125
van Dokkum, P. G. 2001, PASP, 113, 1420
Weidenschilling, S. J. 2002, Icarus, 160, 212